ISSN 0915-633X

NATIONAL INSTITUTE FOR FUSION SCIENCE

High-Beta Discharges with Neutral Beam Injection in CHS

S. Okamura, K. Matsuoka, K. Nishimura, K. Tsumori, R. Akiyama, S. Sakakibara, H. Yamada, S. Morita, T. Morisaki,. N. Nakajima, K. Tanaka, J. Xu, K. Ida, H. Iguchi, A. Lazaros, T. Ozaki, H. Arimoto, A. Ejiri, M. Fujiwara, H. Idei. O. Kaneko, K. Kawahata, T. Kawamoto, A. Komori, S. Kubo, O. Motojima, V.D. Pustovitov, C. Takahashi, K. Toi and I. Yamada

(Received - Apr. 8, 1994)

NIFS-280 May 1994

RESEARCH REPORT
NIFS Series

NAGOYA, JAPAN

High-Beta Discharges with Neutral Beam Injection in CHS

S. Okamura, K. Matsuoka, K. Nishimura, K. Tsumori, R. Akiyama, S. Sakakibara, H. Yamada, S. Morita, T. Morisaki, N. Nakajima, K. Tanaka, J. Xu, K. Ida, H. Iguchi, A. Lazaros [1], T. Ozaki, H. Arimoto [2], A. Ejiri, M. Fujiwara, H. Idei, O. Kaneko, K. Kawahata, T. Kawamoto, A. Komori, S. Kubo, O. Motojima, V. D. Pustovitov [3], C. Takahashi, K. Toi and I. Yamada

National Institute for Fusion Science, Nagoya 464-01, Japan

1) European Community Science and Technology Program

2) Plasma Science Center, Nagoya University, Nagoya 464-01, Japan

3) Permanent address : Kurchatov Institute, Moscow, Russia

Keywords :

CHS, high beta, heliotron/torsatron, self-stabilization, titanium gettering, LHD scaling, magnetic well, Mercier stability, Shafranov shift, position control, magnetic fluctuation

ABSTRACT

High-beta plasmas with a volume-averaged equilibrium beta value 2.1 % were produced in CHS using tangential neutral beam injection. This beta value was achieved with the confinement improvement (reheat mode) observed after turning off a strong gas puffing. The wall conditioning with titanium gettering was used to make a high density operation ($\overline{n_e} < 8 \times 10^{19}$ m^{-3}) possible for low magnetic field (B_t = 0.6 T). The discharges start with the magnetic hill configuration (in vacuum) and finally get Mercier stable equilibrium due to the self-stabilization effect given by the magnetic well which is produced by the plasma pressure. The Shafranov shift was about 40 % of a plasma minor radius. Magnetic fluctuations did not increase with increasing plasma pressure when beta value exceeded 1 %. The dynamic poloidal field control was applied to suppress the outward plasma shift with increasing plasma pressure. Such operation gave an additional increase of beta value compared with the constant poloidal field operation.

1. INTRODUCTION

Beta limit is one of the critical issues in optimizing magnetic field configurations of plasma confinement devices in the fusion research. For heliotron/torsatron devices, the physical mechanism which determines the beta limit depends on the aspect ratio. In large-aspect-ratio design (Heliotron E is one of such systems), the plasma beta is limited by a stability condition [1]. For low-aspect-ratio heliotron/torsatrons, it is possible to raise the stability limit above the equilibrium limit by selecting a proper magnetic field configuration [2]. It is mainly due to the strong self-stabilization effect of magnetic well caused by the large Shafranov shift of magnetic axis. The design policy of ATF, which has a toroidal period number m=12 and plasma aspect ratio $A_p = 8$, was to realize the high beta limit $\langle\beta\rangle = 5\ \%$ in the balance of stability limit and the equilibrium limit condition [3]. They showed experimental results exhibiting self-stabilization effect of finite beta in the discharges with relatively low-beta value $\langle\beta\rangle = 0.5\ \%$ [4,5]. The next generation device LHD ($m = 10$, $A_p = 6.5$) was designed making an optimization for both good confinement and MHD stability [6]. It is shown that the theoretical beta limit in the framework of the ideal interchange stability is 5 % which is limited by the equilibrium condition [7]. In order to realize such high-beta plasmas, the integration of experimental studies on the characteristics of high-beta plasmas is necessary as well as the intensive theoretical work with MHD models. CHS is a comparatively small-size machine with a low aspect ratio ($m = 8$, $A_p = 5$) and it has the theoretical beta limit above 5 % which is at the equilibrium limit [8]. The physical database obtained from high-beta discharges in CHS should make large contribution for understanding special aspects of high-beta plasma performance in low-aspect-ratio configurations.

High-beta experiments in Heliotron E showed average beta value 2 % with a very flat pressure profile [9]. This value was obtained by controlling the pressure profile with a gas puffing to locate the large pressure gradient region near the boundary where the strong shear

stabilization exists. It was claimed that the confinement degradation due to the radiation loss determined the limitation of beta in these experiments. In CHS, the modeling of three-dimensional plasma equilibrium based on the profile measurements (n_e, T_e and T_i) is well formulated [10]. Large Shafranov shift was observed in the profile measurements and it was shown that the observations were in good agreement with the MHD modeling. On the way to realize high-beta plasmas, the MHD equilibrium, stability and the confinement are all important issues. Among them, two questions whether the magnetic surfaces would still exist with a good quality in the configuration near the equilibrium limit, and whether the confinement would be still good for high beta plasmas, are the issues which can be studied mainly in experiments. In the theoretical approaches to the high-beta equilibrium, a new method of computer calculation which does not need to assume the existence of magnetic surfaces has been developed recently [11]. The comparison of experimental results with such a theoretical work is also important. The high-beta discharges in CHS with beta values up to 1.5 % have been analyzed previously [12]. The present paper gives the results of further study for beta range 1.5 - 2.1 %. Because of low aspect ratio, the Shafranov shift in CHS is larger than in any other machine even for the same value of beta. The experimental data related with the equilibrium, stability and confinement of high-beta plasmas would help understanding the physics necessary for next generation machines.

2. EXPERIMENTAL SETUP AND HIGH-BETA DISCHARGES

CHS is a small-size heliotron/torsatron device (toroidal/poloidal mode numbers are $m=8/\ell=2$) which has a nominal major radius (center of helical coils) 1 m and minor radius 0.2 m [8,13]. Maximum magnetic field strength is $B_t = 2$ T. [1] Helical windings have a pitch modulation ($\alpha^* = + 0.3$) which gives larger closed magnetic surfaces and a low aspect ratio ($A_p = 5$). Although the positive pitch modulation is unfavorable for the trapped particle

[1] B_t denotes the magnetic field strength at the geometric axis (R = 1 m).

confinement [14], it enables good access for tangential neutral beam injection in such a small machine as CHS. Two NBI systems are installed in CHS. The NBI-1 was operated with beam energy 40 keV and port-through injection power 1.1 MW. Although injection angle of NBI-1 is variable, the tangential radius of 87 cm was selected for these experiments which gave optimum heating efficiency. Port-through power of NBI-2 was 0.7 MW with 36 keV beam energy and the tangential radius was fixed at 90 cm.

Hydrogen was used for both gas puffing and ion sources of neutral beams. A target plasma for the beam injection was produced by the Nagoya Type-III antenna [15, 16] which gives plasmas for a wide range of magnetic field strength (B_t = 0.55 - 2.0 T) with fixed rf frequency (f = 7.5 MHz). Titanium balls (Mini Ti-Balls) are installed to make titanium gettering for the wall conditioning. Vacuum chamber wall of CHS (stainless steel) is not covered with special protectors (e.g. carbon or light metals) except small carbon tiles installed near the injection port of neutral beams to avoid the direct bombardment by high energy beams on the wall.

Physical characteristics of magnetic surface quantities vary depending on the poloidal field settings (dipole, quadrupole, etc.). The magnetic well structure is primarily determined by the dipole field (or vertical field) which is represented here by the magnetic axis position R_{ax}. The outward shift of magnetic axis (R_{ax} > 97 cm) gives magnetic well while the inward shift gives magnetic hill structure for the vacuum magnetic field configurations. On the other hand, the inward shifted configuration provides better global energy confinement for NBI plasma with co-injection [17, 18], mechanism of which has not yet been understood completely. In high-beta experiments, the R_{ax} = 92 cm configuration was selected in order to assure good global confinement. The polarity of the magnetic field is selected so as to have NBI-1 which gives larger power in co-injection and NBI-2 in counter-injection.

Figure 1 shows the time behavior of the discharge which gave a peak value of (diamagnetic) average beta 2.0 % measured by a diamagnetic loop with a line-averaged electron

density $\overline{n_e} = 6.5 \times 10^{19}$ m^{-3}. The averaged toroidal magnetic field in the plasma was B_{av} = 0.57 T.[2] The absorbed beam power is calculated by a model which is formulated based on the results of Monte Carlo code calculation with HELIOS for co-injection cases using three-dimensional configurations [10, 19]. The heating efficiency for a counter-injection is assumed to be 0.7 times that for a co-injection which is the result of orbit losses of the beam ions hitting on the inboard side vacuum chamber wall. The global energy confinement time of NBI plasmas in CHS generally follows the LHD scaling [20]. It increases as the density increases. But the increase of energy (or confinement time) saturates at a particular level of density, which depends on the heating power and the wall conditioning. When the gas puffing is turned off at such condition, the energy increases rapidly while the density decreases, which is known as the reheat mode [21]. Figure 2 shows such evolution of the discharge in the plotting with the average diamagnetic beta and the density. The global confinement time is 1.7 msec at the maximum beta during the gas puffing and 2.1 msec at the peak of beta in the reheat mode phase. The ratio of the experimental global energy confinement time to the reference value calculated with the LHD scaling (τ_E/τ_{LHD} : $\tau_{LHD} \equiv 0.17\ P^{-0.58}\ \overline{n_e}^{0.69}\ B^{0.84}\ a^2\ R^{0.75}$) is plotted also in Fig. 1. For LHD scaling, P is absorbed power in (MW), $\overline{n_e}$ is the electron density in the unit of (10^{20} m^{-3}), B is magnetic field strength in (Tesla), a and R are the minor and major radii in (m). This confinement time ratio decreases as the density increases which is general tendency of high density plasmas in CHS [18]. The good confinement was recovered with the reheat mode after the gas puffing was turned off.

The contribution of high energy beam component to the pressure profile of NBI plasma which determines the equilibrium is generally large in CHS, while it is relatively small for high density plasmas. The beam pressure is calculated with the PROCTR-MOD code [22] which incorporates the results of beam deposition profile calculation with the Monte Carlo code

[2] B_{av} denotes the averaged value of magnetic field strength in the cross section of equilibrium configuration. The diamagnetic betas are calculated by volume-averaging local beta values.

HELIOS. It is confirmed for many types of discharges that the calculated equilibria with such modeling fit very well to the measured profiles [10]. Although the neutral beam injections are in tangential direction, the diamagnetic beta includes small perpendicular component of beam energy. For the calculation of equilibrium, the larger contribution of parallel beam energy has to be added to the thermal (and perpendicular beam) energies. The estimation of parallel beam energy gives additional beta value of 0.13 % to the diamagnetic beta. Finally the total volume-averaged equilibrium beta is estimated to be 2.1 % which is the highest value obtained so far in helical systems.

3. WALL CONDITIONING AND CONFINEMENT OF HIGH BETA PLASMAS

In the series of high-beta experiments, the plasma beta increased continuously as the titanium gettering was repeatedly made. Thirteen Mini Ti-Balls are installed in the torus. The getter flush covers more than 90 % of vacuum chamber wall surface. Typically ten-minutes flushes are made for every few tens of shots during the high-beta experiments. Short flushes between the discharges are also made in order to keep the plasma parameters constant for the particular sequence of discharges. Figure 3(a) shows the increase of plasma beta as a function of integrated value of titanium gettering on the wall. The port-through NBI power was almost constant (about 1.8 MW total) for all shots plotted in the figure. Open circles are the maximum beta values during the gas puffing (e.g., at 130 msec for the shot shown in Fig. 1) and closed circles are the peak beta values after turning off the gas puffing. The integrated amount of 200 mg/m^2 corresponds to 500 Å thickness of titanium coating in average.

In these shots, the density which gave the highest beta gradually increased as the titanium gettering was repeated. The global energy confinement time also increased with increasing density. In order to check whether the continuous gettering improved the confinement, the ratio of the global energy confinement time to that calculated from the LHD scaling (τ_E/τ_{LHD}) is plotted in figure 3(b). The confinement was improved in the early stage of this series of

experiments but no further improvement (relative to the LHD scaling value) was achieved for the later half while the beta value still increased from 1.7 to 2.0 %.

The beta values are replotted as a function of the average density in Fig. 4(a) from the discharges plotted in Fig. 3. For the data points with gas puffing (open circles), betas are almost proportional to the densities. The beta values larger than 1.7 % were obtained with the reheat mode which appears only for higher densities $\overline{n_e} > 5.5 \times 10^{19}$ m^{-3}. The confinement ratio τ_E/τ_{LHD} is also plotted as a function of the average density in Fig. 4(b). The reheat mode forms different branch of data points from the normal operation data with gas puffing. It is found that the confinement improvement by the reheat mode is about 30 % for good wall conditions. Figure 4(b) does not mean that the confinement ratio is constant for different densities. Because these data are taken from the series of discharges when the continuous effort of wall conditioning was made, the data points for low densities generally correspond to the discharges with insufficient wall condition. The dependence of the confinement ratio on the density for the sufficiently conditioned wall is obtained approximately from Fig. 1 as the time behavior of τ_E/τ_{LHD} with increasing density in a single shot. Similarly, Figure 2 approximately shows the dependence of beta value on the density in a good wall condition.

Figure 5 shows time traces of the diamagnetic beta and magnetic fluctuation signal for the shot in which the beta increased monotonically. The total power (3kHz - 100kHz) of magnetic fluctuation measured by Mirnov coils increased almost proportionally to the plasma beta up to 1 % but it stopped increasing for higher beta value. The fluctuation level in gauss is for the Mirnov coil position. Sixteen magnetic probes are installed in CHS. The signal in Fig. 5 is from the one which is located at a position (top side of the plasma) that is insensitive to the plasma horizontal movement caused by finite beta effects. The dependence of magnetic fluctuation signal on beta is almost similar for all frequency range of the measurement. Such saturation behaviors are common for all shots in high-beta experiments. The collection of data for the shots with various values of beta shows exactly the same dependence of magnetic

fluctuation on beta values [23]. Mirnov signal saturates for the beta range 1 % < ‹β› < 2 %. The coherent mode with m=2/n=1 (m : poloidal mode number / n : toroidal) was observed together with turbulent signal. It increased more rapidly with beta value up to 1 %, while it decreased for higher beta values and finally disappeared for ‹β› > 1.3 %. The 1/1 mode appeared for ‹β› > 0.5 % and it became the largest coherent mode for ‹β› > 1.3 %. Detailed analysis of magnetic fluctuations will be reported in a separate paper [24].

For high-beta experiments, we selected the optimum magnetic field strength so as to obtain a maximum beta value. Such flexibility is available because we have the ICRF target plasma production using Nagoya Type-III antenna. Figure 6 shows the dependence of the plasma average beta on the average magnetic field strength B_{av}. Beta values are plotted both for a fixed average density $\overline{n_e} = 5 \times 10^{19}$ m^{-3} during gas puffing (open circles) and for the time of peak beta in the reheat mode (closed circles). Both data show maximum beta in the range of average magnetic field strength B_{av} = 0.55 - 0.59 T. Near this optimum field, the global confinement time should scale as $\tau_E \propto B_{av}^{\,2}$ because the beta scales as $\langle\beta\rangle \propto B_{av}^{\,-2}$. In advance to the high-beta experiments, the dependence of global energy confinement time was studied for the plasma density range $\overline{n_e} < 4 \times 10^{19}$ m^{-3} using a single co-injection NBI with the port through injection power 0.5 - 0.6 MW. For the purpose of extracting the dependence of global confinement time on the magnetic field strength, τ_E is normalized for different values of absorbed power and plasma density assuming that dependencies on those parameters follow the LHD scaling. The dependence factor on the magnetic field strength defined by

$$F_B \equiv \tau_E \,/\, 0.17\, P^{-0.58}\, \overline{n_e}^{\,0.69}\, a^{\,2}\, R^{\,0.75}$$

was calculated for all data in the density range $\overline{n_e} = 2 - 4 \times 10^{19}$ m^{-3}. The averaged value of F_B for the different magnetic field strength are plotted in Fig. 7. The data for the magnetic field strength higher than 0.8 T give the B dependence factor $F_B = 0.95 \times B_{av}^{\,0.75}$. It is clear that F_B for 0.58 T does not follow such a scaling, and τ_E for the magnetic field strength around 0.58 T

should depend on the field strength with a larger power value than 0.75. It is consistent with the result obtained from Fig. 6.

4. DETERMINATION OF PLASMA BOUNDARY AND DYNAMIC POLOIDAL FIELD CONTROL

It is important to study the behavior of plasma boundary for high-beta discharges based on the measurements in experiments. Standard MHD theories would give us the variation of a boundary shape for a high-beta equilibrium but it is under the assumption of the existence of good magnetic surface at the boundary. Completeness of magnetic surfaces for high-beta plasmas can be confirmed only by the experimental measurements. As will be discussed in Sec. 5, it is expected that the center of the last closed flux surface (LCFS) moves about 1 cm outward when the plasma beta reaches 2 %. Such shift of plasma position changes both MHD stability characteristics and the confinement. A dynamic poloidal field control during the discharge was made to fix the plasma boundary position unchanged when the plasma beta increases. Benefits of such position control was pointed out from the theoretical point of view in obtaining high-beta plasmas when the plasma beta value approaches the equilibrium limit [25]. This method is also useful in technical sense when it is requested to fix the plasma boundary during high-beta discharges from the aspect of interference between the plasma boundary and plasma periphery structures such as limiters or divertors.

Figure 8 shows a time sequence of high-beta discharge with the poloidal field control. The current settings for the poloidal coils were changed during the discharge from those for the configuration with R_{ax} = 92 cm to those for R_{ax} = 90 cm in order to push back LCFS to the inward direction. This dynamic change of poloidal coil current made 0.2 - 0.3 volt one-turn voltage[3] which caused 2 - 3 kA increase of the plasma current in a counter direction. But it is

[3] It is possible to make no one-turn voltage by selecting another combination of poloidal coil currents. The current settings chosen in these experiments were for the condition of minimum stray field in the vicinity of the machine.

known from the experiments that this level of plasma current does not make significant effects on the global confinement in CHS. In the three-dimensional equilibrium calculation, the position of the LCFS at $\langle\beta\rangle = 1.5$ % with poloidal field setting for $R_{ax} = 90$ cm is almost the same as the position of the vacuum LCFS for $R_{ax} = 92$ cm configuration (difference is less than 0.1 cm).

In order to confirm whether the plasma position control was successful, the position of the plasma boundary at the outboard side was determined by the VUV profile measurements with rotating mirror system (total emission in the range 400 Å ~ 1800 Å including dominant contribution of Lyman α was detected [26]) and the density profile measurements using a lithium beam probe [27] at the plasma boundary. The VUV profiles were measured at the toroidal position where the magnetic surfaces are vertically elongated, while the lithium beam probe diagnostics gives the edge density profiles at the toroidal position where the magnetic surfaces are horizontally elongated. Because the plasma edge at the inboard side for $R_{ax} = 92$ cm configuration is fixed by the inner wall acting as a toroidal limiter, positions of LCFS can be determined from the measurement of the outboard side boundary.

Figure 9(a) shows the time evolution of outboard side VUV emission profile for the discharge with no poloidal field control. As well as the emission level increased with the almost monotonical increase of plasma density, the boundary moved outward with the increase of beta. When the dynamic poloidal field control was applied, such outward shift of the plasma boundary was suppressed as is shown in Fig. 9(b). The edge positions measured by the lithium beam probe gave the similar results for two discharges which are shown in Fig. 10(a) and (b). At the toroidal cross section where the plasma is horizontally elongated, the distances between magnetic surfaces near boundary are relatively expanded at the midplane which makes the determination of plasma boundary unclear. The lithium beam is injected from the outboard side bottom position where the plasma boundary is much clearer. The horizontal axis in Fig. 10 is the distance along the lithium beam injection.

Because in our experiments the poloidal field control was not flexible for its time programming, it was possible to keep the plasma boundary position unchanged only for a part of full discharge time. When we compare the average beta values of two shots for the same densities, the discharge with poloidal field control gave about 10 % additional beta to that in no control case. The difference of betas appeared at 70 msec and increased gradually till 130 msec. For this time period, the plasma boundary position was kept almost constant with the poloidal field control. The total plasma energy for the same density was about the same for two cases. It is because the plasma volume did not increase due to the suppression of the shift of LCFS when the position control was applied. The Mirnov signals were roughly 1.5 times higher for the poloidal-field-control case compared with no-control case in the saturation level for $\langle\beta\rangle > 1$ %. In the reheat mode, the plasma beta changes very quickly. So the poloidal field control is difficult to keep the plasma position unchanged. In addition, the optimization of gas puffing time programming is necessary in order to get a large improvement factor with reheat mode. The additional increase of beta with the poloidal field control for the reheat mode was not obtained in these experiments.

5. DISCUSSIONS

The global energy confinement times in CHS high-beta discharges are lower than the values that the LHD scaling gives as is shown in Fig. 3(b) and 4(b). It is a simple result when we select the optimum conditions for the magnetic field and the plasma density in order to get high-beta plasmas. Since the plasma beta is proportional to $1/B^2$ and the global energy confinement scales with $B^{0.75}$ for high magnetic field strength (Fig. 7), the maximum beta is obtained at low magnetic field for which the confinement does not follow such scaling dependence. Similar situation occurs for the optimum density for the high-beta discharge. Since the LHD scaling shows that the confinement is proportional to $\bar{n}_e^{0.69}$, the plasma density

which gives maximum beta (energy) is the one at which the confinement does not increase any more. These are the main reasons why the scaling ratio (τ_E/τ_{LHD}) in high-beta discharges in CHS is about 0.6. The improvement with reheat mode compensates the density degradation near the high density limit. But the scaling ratios with the reheat mode still remain to be about 0.8. This is supposed to come from the deviation of the global confinement scaling from the LHD scaling for low magnetic field. The scaling ratio 0.8 shown in Fig. 4(b) is the similar value to the scaling ratio found in Fig. 7 for $B_{av} = 0.58$ T.

The progress of average beta values in this experiment was brought by the effort to increase the densities which gave maximum plasma betas. The obtained beta values are almost proportional to the densities as is shown in Fig. 4(a). The additional increases of beta were obtained with the confinement improvement due to the reheat mode which is about 30 %. The density which gave beta maximum during gas puffing for good wall condition was about 60 % of the density limit scaling for helical systems : $n_e^S \equiv 0.25\ (P\ B/a^2\ R)^{0.5}$ [20] where the parameters are in the same units as in the LHD scaling for the global confinement time.

Since the plasma energy does not increase as much as the density shown in Fig. 1, the temperature generally decreases as the density increases in our experiments. The beta maximum is obtained at the density above which the temperature drops more rapidly with increasing density. In terms of temperature, there is a critical temperature below which the confinement degrades rapidly. The ratios of the maximum beta (energy) to the density give average values of such critical temperature. The fact that the peak betas were proportional to the densities during the progress of the wall conditioning means that the critical temperature did not change in this series of experiments. The improvement of the confinement with the wall conditioning increased the temperature for the given density which increased the maximum density corresponding to the critical temperature. As is noted in Sec. 3, Fig. 4(b) does not mean that the confinement was not improved during the series of experiments. This figure gives the acceptable degradation level of the confinement ($\tau_E/\tau_{LHD} = 0.6$) for the densities

which give maximum betas for each stage of wall conditioning.

It was reported that no degradation of global confinement time directly caused by beta value itself was found for high-beta discharges in CHS for $\langle\beta\rangle < 1.5$ % [12]. In this series of experiments, the conclusion was confirmed for beta values up to $\langle\beta\rangle \leq 2.1$ %. It was possible to increase the maximum beta value day by day with only the continuous wall conditioning while the port-through NBI heating power was almost at the same level thoughout. The sufficient level of global confinement time ratio ($\tau_E/\tau_{LHD} = 0.8$) for the reheat mode was achieved for higher beta discharge by the improvement of wall conditioning.

The finite-beta equilibria were calculated using the free-boundary VMEC code [28] which should correspond to the real experimental conditions without vertical field control during discharges. Vacuum field was calculated with MAGN code [29] which allows to take into account of finite dimensions of the coils. Because the pressure profile is important for the equilibrium calculation, the complete information of measured profiles for the electron density and the electron and ion temperatures are used in constructing the reference pressure profile for the discharge with 0.7 % average equilibrium beta and line-averaged density $\overline{n_e} = 3 \times 10^{19}$ m^{-3}. Since the shift of the magnetic axis due to the finite plasma pressure is significant for the low-aspect-ratio helical systems like CHS, the procedure of iterative calculation for the equilibrium and the measured pressure profile fitting was made to get final equilibrium [10]. The high-energy beam pressure was included in the equilibrium calculations. The resultant pressure profile is $p_{eq}(r) = 1.71\ (1-(r/a)^{1.7})^{1.5} \times 10^{19}$ eV m^{-3}. It is more peaked than the thermal pressure profile without beam component which fits to $p_{th}(r) = 1.04\ (1-(r/a)^{2.1})^{1.5} \times 10^{19}$ eV m^{-3}. The profile $p_{eq}(r)$ turns out to have a very similar shape to the profile $(1-(r/a)^2)^2$ which is widely used for the model calculation assuming parabolic profiles for both density and temperature. The $p_{eq}(r)$ has a larger gradient than the parabolic one only near the boundary $r/a > 0.8$. Because the profile measurements are not available for all beta values, the same pressure profile $p_{eq}(r)$ was used for the equilibrium calculations in the range of beta $0\ \% \leq \langle\beta\rangle \leq 2\ \%$. Figure 11(a) shows the profiles of the rotational transform ι for selected average beta

values $\langle\beta\rangle = 0$ %, 0.5 %, 1 % and 2 %. The rotational transform at the edge increases from 1.03 (vacuum case) to 1.25 when $\langle\beta\rangle$ reaches 2 %. The magnetic well is shown in Fig. 11(b). The configuration with magnetic axis position $R_{ax} = 92$ cm has magnetic hill in vacuum, but the magnetic well is formed by the plasma pressure for large area $r/a < 0.7$ when $\langle\beta\rangle$ becomes 2 %.

As was noted in Sec. 2, the magnetic field configuration with $R_{ax} = 92$ cm was selected in high-beta experiments because it gives the best global confinement for co-injection NBI taking less account of the MHD stability (outward shifted configuration has better stability characteristics due to the magnetic well). Because this configuration is inward shifted one, the LCFS is determined by the inboard side vacuum wall acting as a toroidal limiter. In the equilibrium calculation, the toroidal flux values were given so as that the plasma boundary should be determined by the inboard side vacuum wall[4]. When the plasma beta increases, the LCFS shifts to outboard side thus making the plasma volume larger. The increase of the rotational transform at the edge for the high-beta configuration is mainly due to this effect. Figure 12 shows the shift of the center of LCFS (at the toroidal cross section where the magnetic surfaces are vertically elongated) and increase of plasma volume as functions of average beta. The calculated values of the ratio of the average shift of magnetic axis (relative to the center of LCFS) to the average minor radius are also plotted. Because the $R_{ax} = 92$ cm configuration is an inward shifted one, this ratio starts from the negative value at $\langle\beta\rangle = 0$ %. The magnetic axis position for the vacuum configuration with the same LCFS position as the $\langle\beta\rangle = 2$ % equilibrium is $\Delta/a \sim 0.02$. So the value $\Delta/a \sim 0.4$ for $\langle\beta\rangle = 2$ % is mostly from the Shafranov shift. If we assume that a half of minor radius gives the practical limit of high-beta equilibrium, the shift of magnetic axis for the average beta 2 % should be about 80 % of that

[4] For the outward shifted configuration, the plasma boundary formed by the separatrix is detached from the vacuum chamber wall. But the configurations in vacuum with the same LCFS positions as the high beta plasmas in this experiments are still limited by the inner wall.

limit.

The position of the outboard side plasma boundary given by the VMEC code calculation for $\langle\beta\rangle = 0$ % is 106.8 cm, which can be compared with the profiles in Fig. 9. Because the inboard side boundary is almost fixed at the vacuum chamber wall, the calculated shift of outboard side boundary with finite beta is about two times of LCFS shift shown in Fig. 12. The positions of boundary given by the equilibrium calculation roughly correspond to the upper edge of the VUV profiles. The VUV emission area expanded more than the calculated boundary position. It is generally observed for high density plasmas in CHS. The poloidal field control pushed back such expansion as a whole. As for the lithium beam probe diagnostics, the calculated boundary position in vacuum configuration for Fig. 10 is 11.6 cm. It moves to 13 cm for $\langle\beta\rangle = 1$ % and 13.3 cm for $\langle\beta\rangle = 1.5$ %. Because the beta increased more slowly than the increasing density for these experiments, the shift of the boundary in Fig. 10 (when the positions for the same densities are compared) is larger than the calculated equilibrium boundary shift. The time variation of poloidal field control fitted to suppress such shift of boundary. Because two boundary measurements give mainly density profile information, the discussions about the pressure profile cannot be made for these experiments. But the assumption made in Sec. 4 that the finite beta plasma boundary was determined by the inboard side wall acting as a limiter is confirmed by these measurements.

Based on the equilibria shown in Fig. 11, the Mercier criterion is calculated. Figure 13 shows a contour map of the Mercier criterion normalized to the shear stabilization term defined as $D_I \equiv - D_M/\iota'^2$, where D_M is the standard Mercier criterion [7]. As Fig. 11(b) shows, vacuum magnetic configuration with $R_{ax} = 92$ cm has a magnetic hill everywhere. But the magnetic well is produced for $\langle\beta\rangle \geq 0.3$ %. Figure 13 shows that the equilibrium with beta value more than 1.3 % becomes Mercier stable. It is widely accepted that the MHD stability for the low n mode determines the actual threshold for the stability of laboratory plasmas. From the comparison between the Mercier criterion calculation and the low-mode ideal interchange

stability calculation, the practical criterion $D_I < 0.2$ was proposed for the evaluation of the MHD stability for the low-mode ideal interchange instabilities [30]. From such a viewpoint, the beta value higher than 0.7 % is sufficient for the stability of the interchange mode in these experiments. Since the measured pressure profile for 0.7 % is used for the equilibrium calculations, the Mercier stability calculation for the beta value around 0.7 % should be reliable for the description of the experiment.

There is a possibility that the thermal pressure profiles for high-beta discharges ($\langle\beta\rangle > 1.5$ %) were more peaked than those for $\langle\beta\rangle = 0.7$ %, because these data were taken with reheat mode which normally has relatively peaked density profiles [21]. The profile measurement of visible bremsstrahlung gave very peaked density profile for high-beta discharges with the assumption that Zeff is uniform in the plasma. If we take this peaked density profile assuming parabolic temperature profiles, the central beta exceeds 7 % for the discharge with 2.1 % equilibrium beta. But the density and temperature profile data have not been obtained for those discharges.

In spite of the fact that the low-beta plasma has the region where the Mercier criterion is not satisfied, the global confinement characteristics of the real laboratory plasma did not show detectable reflection of such MHD instability. But there is coincidence between the dependence of the magnetic fluctuations on beta value (Fig. 5) and the ideal interchange stability diagram (Fig. 13). Though the mechanism for the fluctuations which gave those Mirnov signals has not been completely identified in CHS, the strong MHD stabilization effect of self-induced magnetic well should be the cause for the beta dependence of the magnetic fluctuation signals.

If we check the position of the rational surfaces for the low-mode resonances in Fig. 13 and consider that the practical stability criterion is $D_I < 0.2$, the dangerous rational surfaces stay only in the region $r/a < 0.5$. It can be the reason why we did not observe large degradation effects of MHD instability in the global performance of the plasma. For the configuration with more inward shifted magnetic axis (e.g. $R_{ax} = 90$, 89 cm), the Mercier stability condition

becomes worse even for higher beta values (self-stabilization effect is much less than in the case with R_{ax} = 92 cm). The global confinement shown in the experiments is still not significantly bad for such inward shifted case compared with R_{ax} = 92 cm, though we observed MHD activities in the soft X-rays and Mirnov signals for the counter-injection NBI plasma in the R_{ax} = 89 cm configuration.

The experiments with dynamic poloidal field control gave us another example for the relation between the global plasma performance and the ideal MHD stability criterion in heliotron/torsatron machines. Although the pushed-back equilibrium with the poloidal field control had much wider Mercier unstable region [5], the apparent average beta was even better for the poloidal-field-control case than for no-control case which has a much better Mercier stability due to the magnetic well stabilization. However the Mirnov signals were larger for the poloidal-field-control case which is expected by the stability calculations. For further discussions, more informations about the profile measurements are necessary as well as the fluctuation data for various configurations and beta values. CHS is very convenient machine for the direction of such studies because of its flexibility of magnetic field configuration and the wide operational area of plasma betas.

The expected Shafranov shift was about 40 % of an average minor radius for the high-beta discharges in this experiments. The plasma boundary position was measured by the VUV profile measurements for all shots in the experiments and no single shot has been found which shows the reduction of plasma radius compared with the equilibrium calculations using the free-boundary VMEC code with the assumption that the outermost magnetic surface determined by the inner wall limiter exists. The calculated value of ι at the boundary increased from 1.03 to 1.25 with the expansion of the plasma volume due to the outward shift of LCFS by the

[5] The calculation of Mecier stability criterion for the fixed boundary equilibrium shows that the average beta value necessary for the Mercier stability is more than 2 %. The realized equilibrium in the dynamic poloidal field control experiments should be inbetween such fixed boundary equilibrium and the free boundary equilibrium.

plasma pressure. The good correspondence of the boundary positions both in the measurement and in the calculations means that magnetic surfaces with iota value above unity still exist clearly even for high-beta plasmas up to 2 %. The observation of 1/1 coherent mode in Mirnov signals for the beta range $\langle\beta\rangle > 0.5$ % confirms also the confinement of finite plasma pressure in the boundary region with $\iota > 1$.

6. CONCLUSION

The volume-averaged equilibrium beta value 2.1 % was achieved in CHS with hydrogen plasmas which is the highest value obtained so far in helical systems. Two neutral beams in tangential injection (port-through power : P = 1.8 MW) were used for producing high density plasma (line-averaged density : $\overline{n_e} = 6.5 \times 10^{19}$ m^{-3}) in the low magnetic field operation (averaged magnetic field strength : $B_{av} = 0.57$ T). The ICRF target plasma was produced with Nagoya Type-III antenna. Titanium gettering was used for the wall conditioning. The beta increased in proportional to the density as the wall condition improved. The reheat mode after the turning off gas puffing gave additional increase of beta by 30 %. Ratios of the global energy confinement time to the LHD scaling value (τ_E/τ_{LHD}) were 0.6 for the discharges with continuous gas puffing and 0.8 for the reheat mode.

The dynamic poloidal field control suppressed the outward shift of the plasma boundary caused by the finite plasma pressure. The fixing of boundary position was confirmed by two methods of plasma edge diagnostics (VUV profile measurement and lithium beam probe). The poloidal field control operation gave about 10 % additional beta increase.

The magnetic fluctuation measurement with Mirnov coils showed the increase of fluctuations almost in proportional to the beta value for the beta range $0\ \% < \langle\beta\rangle < 1\ \%$ and the saturation of signals for the beta range $1\ \% < \langle\beta\rangle < 2\ \%$. No degradation of the global energy confinement was observed for the beta value up to 2 %.

ACKNOWLEDGEMENTS

The authors are grateful to the continuous support given by the Director-general A. Iiyoshi and the director T. Kuroda in National Institute for Fusion Science. They thank also to Messrs. S. Hattori, K. Kobayashi and K. Seko for their technical support in the operation of NBI systems.

REFERENCES

[1] WAKATANI, M., et al., Nucl. Fusion **26** (1986) 1359.

[2] CARRERAS, B.A., et al., Nucl. Fusion **28** (1988) 1195.

[3] CARRERAS, B.A., et al., Phys. Fluids **26** (1983) 3569.

[4] HARRIS, J.H., et al., Phys. Rev. Lett. **63** (1989) 1249.

[5] HARRIS, J.H., et al., Phys. Fluids **B 2** (1990) 1353.

[6] IIYOSHI, A., et at., Fusion Technol. **17** (1990) 169.

[7] ICHIGUCHI, K., et al., Nucl. Fusion **33** (1993) 481.

[8] NISHIMURA, K., et al., Fusion Technol. **17** (1990) 86.

[9] MOTOJIMA, O., et al., Nucl. Fusion **25** (1985) 183.

[10] YAMADA, H., et al., Nucl. Fusion **32** (1992) 25.

[11] HAYASHI, T., et al., Phys. Fluids **B 4** (1992) 1539.

[12] YAMADA, H., et al., in Plasma Physics and Controlled Nuclear Fusion Research 1992 (Proc. 14th Int. Conf. Würzburg, 1992), Vol. 2, IAEA, Vienna (1993) 493.

[13] MATSUOKA, K., et al., in Plasma Physics and Controlled Nuclear Fusion Research 1988 (Proc. 12th Int. Conf. Nice, 1988), Vol. 2, IAEA, Vienna (1989) 411.

[14] OKAMURA, S., et al., in Plasma Physics and Controlled Nuclear Fusion Research 1992 (Proc. 14th Int. Conf. Würzburg, 1992), Vol. 2, IAEA, Vienna (1993) 507.

[15] WATARI, T., et al., Phys. Fluids **21** (1978) 2076.

[16] OKAMURA, S., et al., Nucl. Fusion **26** (1986) 1491.

[17] OKAMURA, S., et al., Effect of magnetic axis shift of CHS plasma characteristics, in Next Generation Experiments in Helical Systems (Proc. 1st Int. Toki Conf., 1989), NIFS-PROC-3 (1990) 224.

[18] KANEKO, O., et al., in Plasma Physics and Controlled Nuclear Fusion Research 1990 (Proc. 13th Int. Conf. Washington, 1990), Vol. 2, IAEA, Vienna (1991) 474.

[19] HANATANI, K., PENNINGSFELD, F.P., Nucl. Fusion **32** (1992) 1769.

[20] SUDO, S., et al., Nucl. Fusion **30** (1990) 11.

[21] MORITA, S., et al., in Plasma Physics and Controlled Nuclear Fusion Research 1992 (Proc. 14th Int. Conf. Würzburg, 1992), Vol. 2, IAEA, Vienna (1993) 515.

[22] HOWE, H.C., et al., in Controlled Fusion and Plasma Physics (Proc. 16th Eur. Conf. Venice, 1989), Vol. 13B, Part II, European Physical Society, Geneva (1989) 683.

[23] MATSUOKA, K., et al., High-beta experiment and confinement regimes in CHS, submitted to Fusion Engineering and Design.

[24] SAKAKIBARA, S., et al., Magnetic fluctuations in CHS plasma, to be submitted to J. Plasma and Fusion Res..

[25] PUSTOVITOV, V.D., Comments Plasma Phys. Control. Fusion, **15** (1992) 121.

[26] MORITA, S., et al., Topological edge layer studies of ECH and NBI plasmas in CHS, in Stellarators and Other Helical Confinement Systems (Proc. 9th Int. Workshop on Stellarators, 1993), IAEA, Vienna (1993) 542.

[27] MORISAKI, T., et al., Edge plasma measurememts in the compact helical system (CHS) with a thermal neutral beam probe, to be submitted to J. Phys. Soc. Jpn..

[28] HIRSHMAN, S.P., et al., Comput. Phys. Commun. **43** (1986) 143.

[29] TODOROKI, J., J. Phys. Soc. Jpn. **58** (1989) 3979.

[30] NAKAMURA, Y., et al., J. Phys. Soc. Jpn. **58** (1989) 3157.

Figure Captions

Fig. 1 Time behavior of high-beta discharge : Line-averaged density, gas puffing rate, diamagnetic average beta, NBI absorbed power, ratio of global energy confinement time to the LHD scaling (τ_E/τ_{LHD}).

Fig. 2 Time evolution of diamagnetic average beta and line-averaged density. Square points show time intervals of 5 msec.

Fig. 3 (a) Diamagnetic average beta and (b) ratio of global confinement time to the LHD scaling (τ_E/τ_{LHD}) as functions of integrated titanium sublimation. Open circles are for maximum beta values during gas puffing, while closed circles are for peak beta values in reheat mode.

Fig. 4 (a) Diamagnetic average beta and (b) ratio of global confinement time to the LHD scaling (τ_E/τ_{LHD}) as functions of line-averaged density. Open circles are for maximum beta values during gas puffing, while closed circles are for peak beta values in reheat mode.

Fig. 5 Time traces of diamagnetic beta and magnetic fluctuation signal in the range of 3 to 100 kHz. The amplitudes of fluctuation (in gauss) are at magnetic probe position.

Fig. 6 Dependence of diamagnetic average beta on the average magnetic field strength. Closed circles show peak beta values in reheat mode and open circles show beta values at the same average density $\overline{n_e} = 5 \times 10^{19}$ m^{-3} with gas puffing.

Fig. 7 B dependence factor (normalized τ_E) as a function of average magnetic field strength. Closed circle for $B_{av} = 0.58$ T is not on the power scaling formed by other points.

Fig. 8 Relative timing of dynamic poloidal field control to the plasma discharge. Currents in three poloidal coils are varied during discharge from the settings for $R_{ax} = 92$ cm vacuum field configuration to the settings for $R_{ax} = 90$ cm configuration.

Fig. 9 Time evolutions of VUV emission profiles for (a) no poloidal field control and (b) dynamic poloidal field control.

Fig. 10 Time evolutions of edge density profiles measured with lithium beam probe for (a) no poloidal field control and (b) dynamic poloidal field control.

Fig. 11 Radial profiles of (a) rotational transform, (b) magnetic well obtained from free-boundary VMEC equilibrium calculations for $R_{ax} = 92$ cm configuration. Four selected equilibria are plotted for $\langle\beta\rangle = 0$ %, 0.5 %, 1 % and 2 %. Pressure profile is assumed to be proportional to $p(0)\,(1-(r/a)^{1.7})^{1.5}$ for each equilibrium.

Fig. 12 Calculated values of expansion of plasma volume, shift of last closed flux surface (LCFS) at the toroidal position where the magnetic surfaces are vertically elongated and the ratio of magnetic axis shift to minor ratius (Δ/a) as functions of average beta.

Fig. 13 Contour map of normalized Mericier stability criterion D_I obtained from free-boundary VMEC equilibrium calculations for $R_{ax} = 92$ cm configuration. Thick solid line gives Mercier stability boundary : $D_I = 0$. Thinner lines give contours with steps $\Delta D_I = 0.2$.

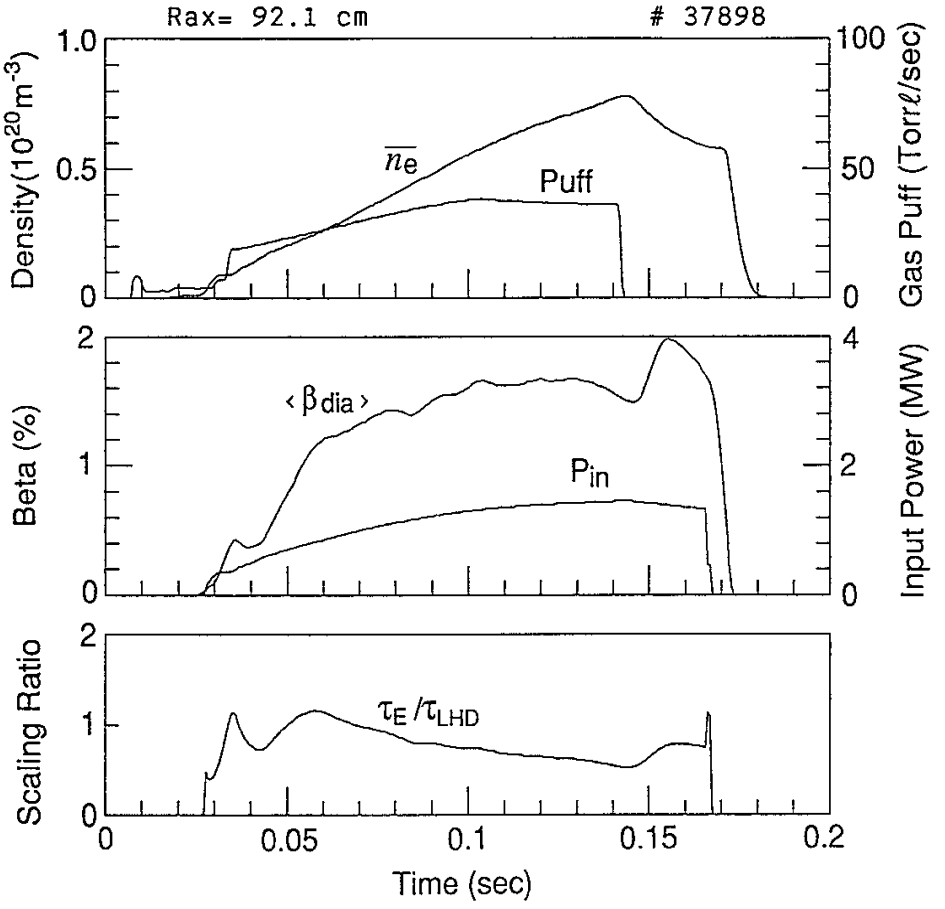

Fig. 1 Time behavior of high beta discharge : Line-averaged density, gas puffing rate, diamagnetic average beta, NBI absorbed power, ratio of global energy confinement time to the LHD scaling (τ_E/τ_{LHD}).

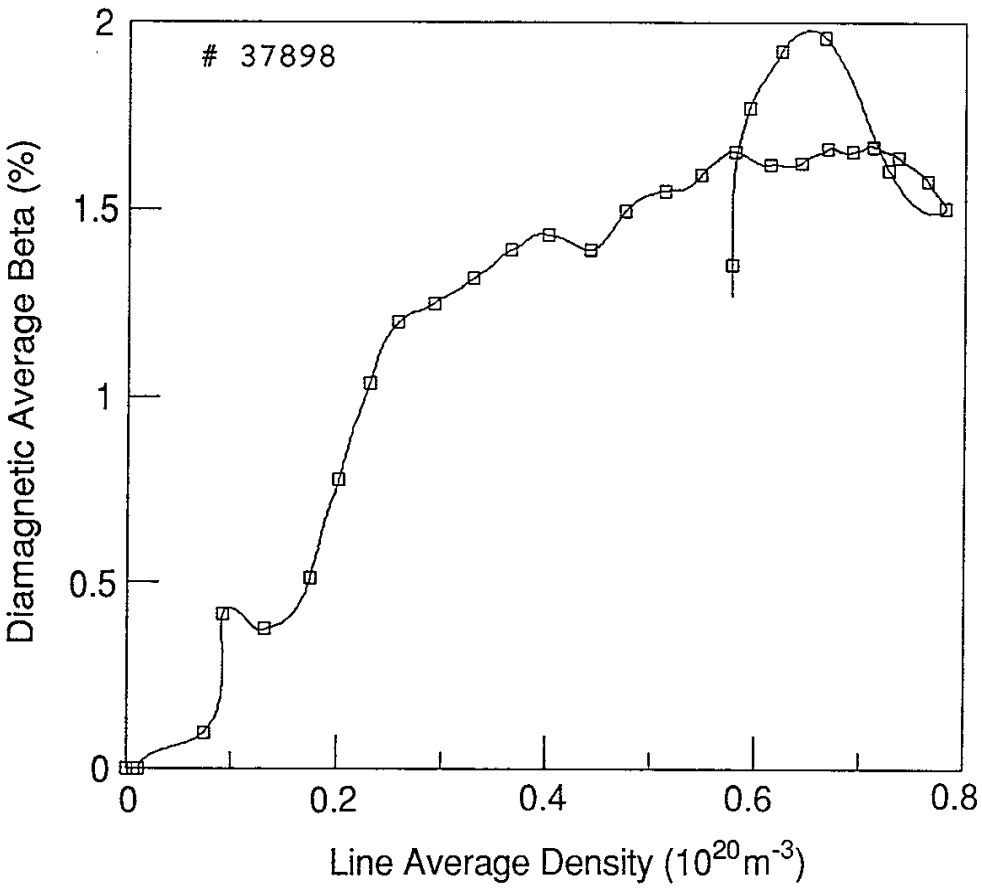

Fig. 2 Time evolution of diamagnetic average beta and line-averaged density. Square points show time intervals of 5 msec.

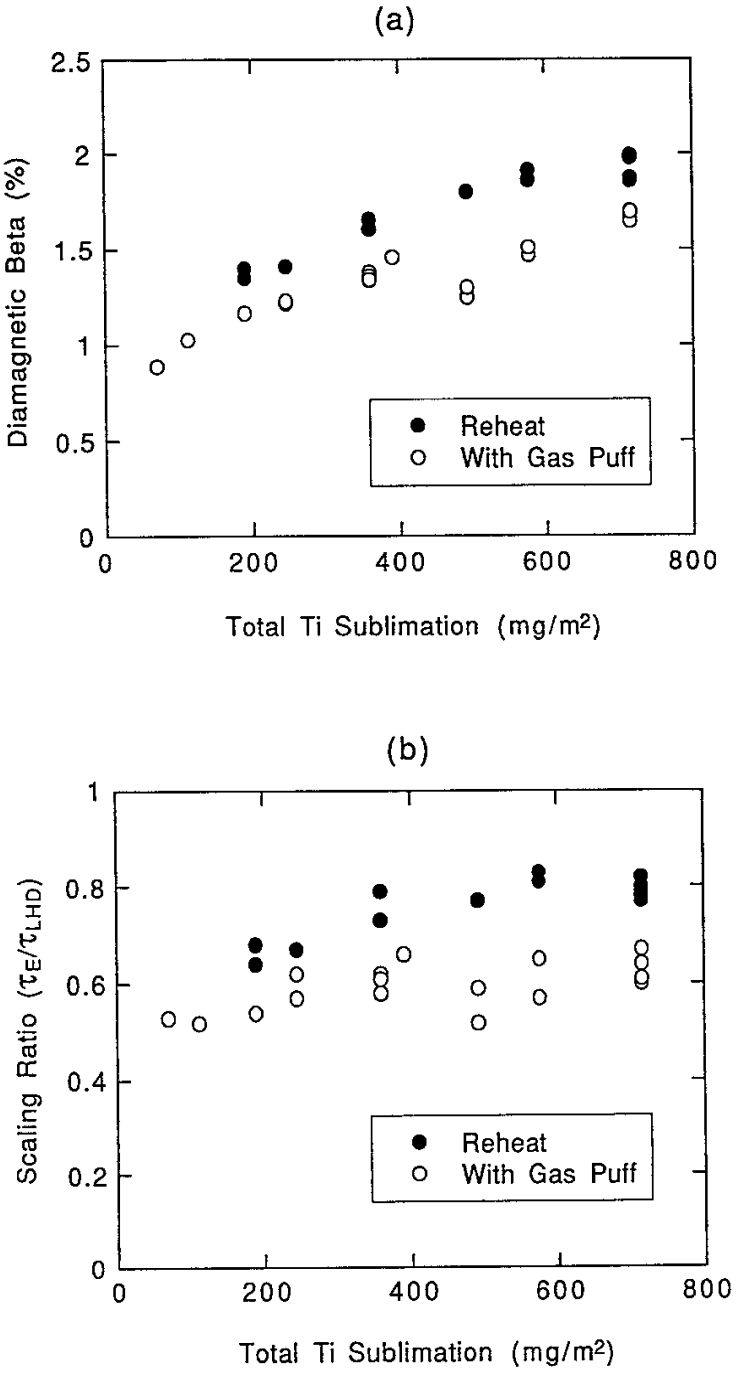

Fig. 3 (a) Diamagnetic average beta and (b) ratio of global confinement time to the LHD scaling (τ_E/τ_{LHD}) as functions of integrated titanium sublimation. Open circles are for maximum beta values during gas puffing, while closed circles are for peak beta values in reheat mode.

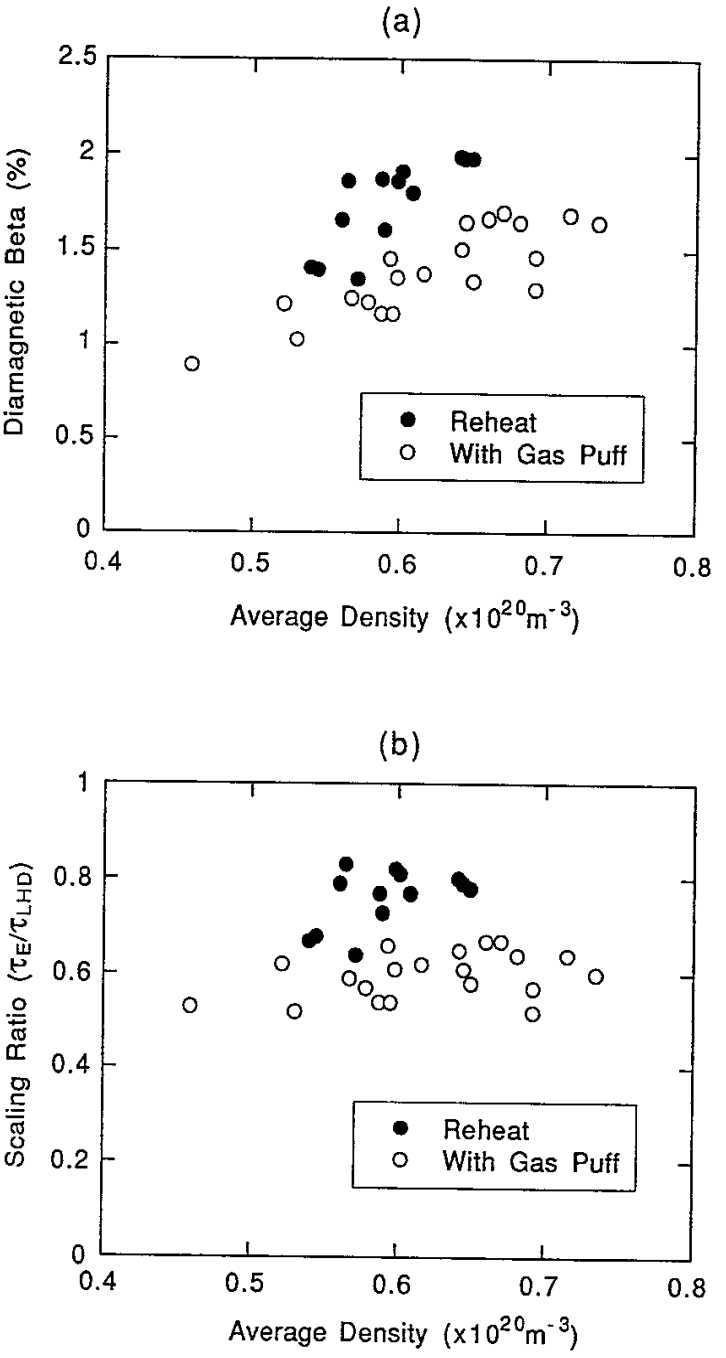

Fig. 4 (a) Diamagnetic average beta and (b) ratio of global confinement time to the LHD scaling (τ_E/τ_{LHD}) as functions of line-averaged density. Open circles are for maximum beta values during gas puffing, while closed circles are for peak beta values in reheat mode.

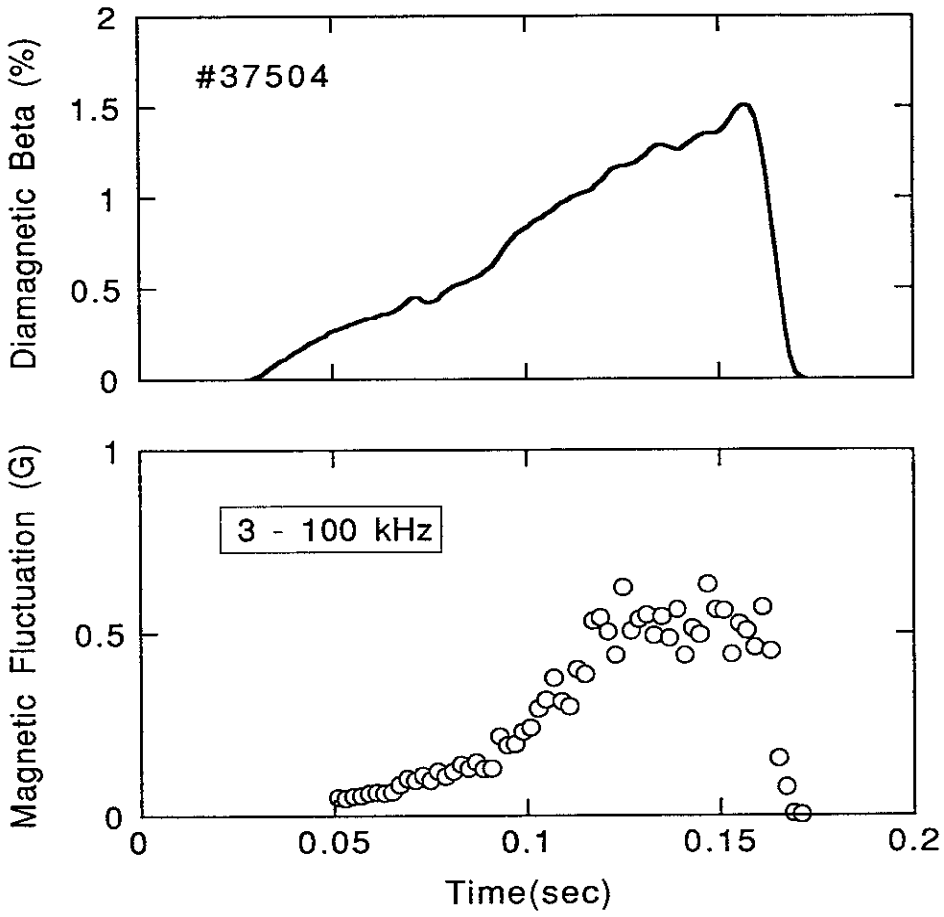

Fig. 5 Time traces of diamagnetic beta and magnetic fluctuation signal in the range of 3 to 100 kHz. The amplitudes of fluctuation (in gauss) are at magnetic probe position.

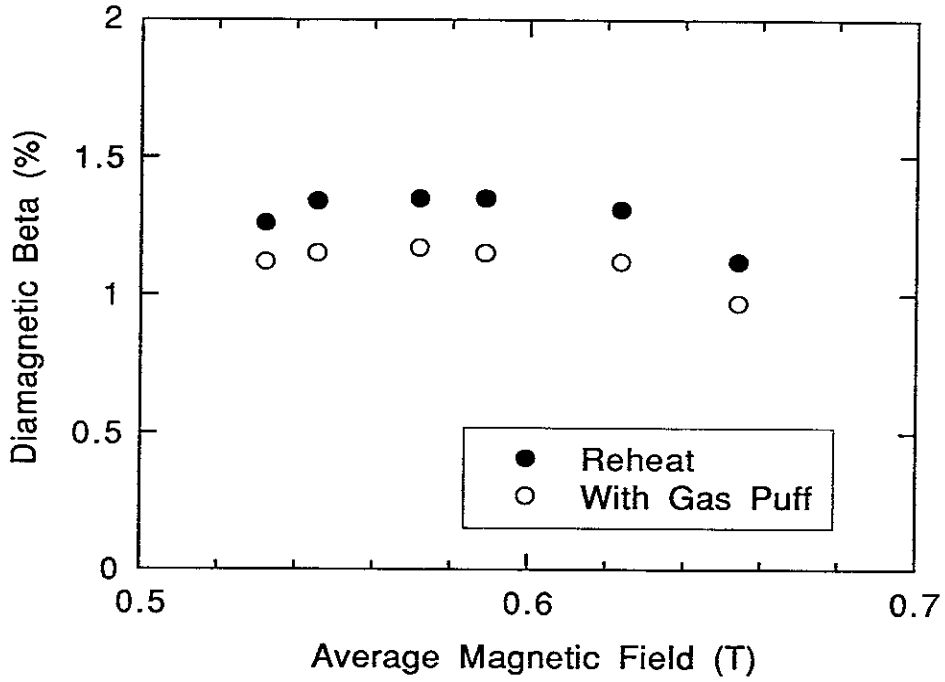

Fig. 6 Dependence of diamagnetic average beta on the average magnetic field strength. Closed circles show peak beta values in reheat mode and open circles show beta values at the same average density $\bar{n_e} = 5 \times 10^{19}$ m^{-3} with gas puffing.

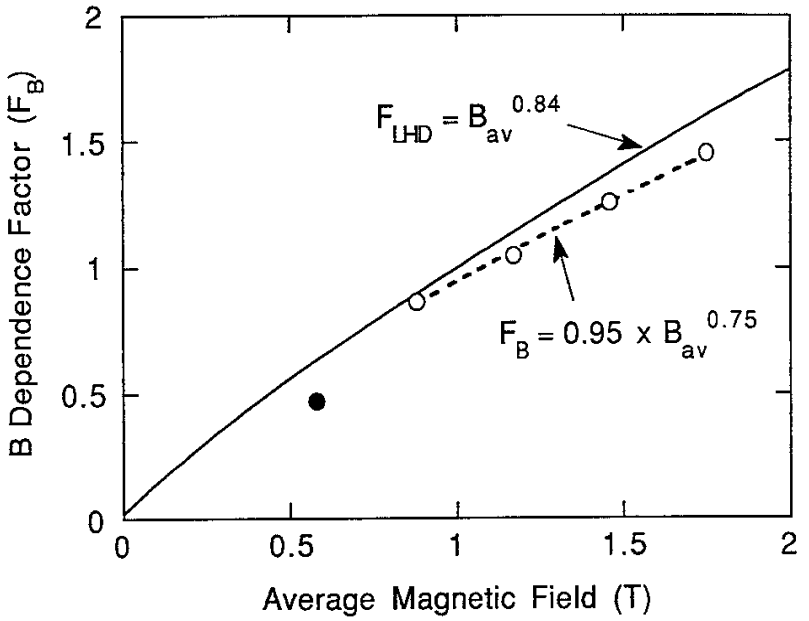

Fig. 7 B dependence factor (normalized τ_E) as a function of average magnetic field strength. Closed circle for $B_{av} = 0.58$ T is not on the power scaling formed by other points.

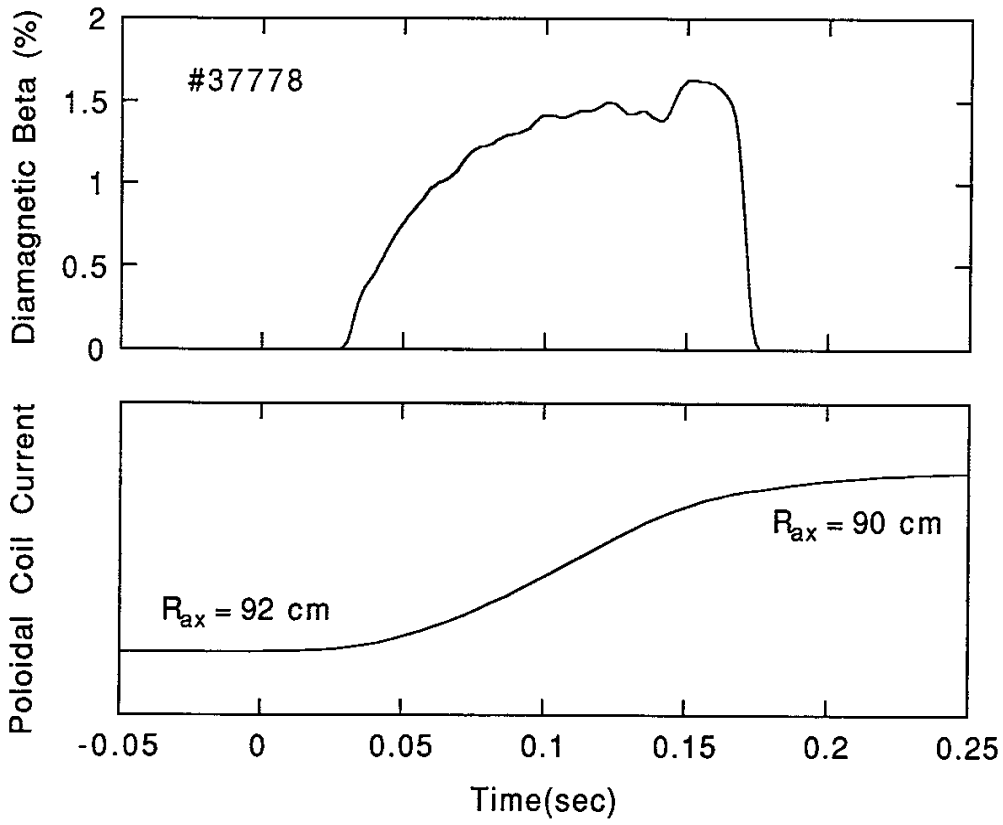

Fig. 8 Relative timing of dynamic poloidal field control to the plasma discharge. Currents in three poloidal coils are varied during discharge from the settings for $R_{ax} = 92$ cm vacuum field configuration to the settings for $R_{ax} = 90$ cm configuration.

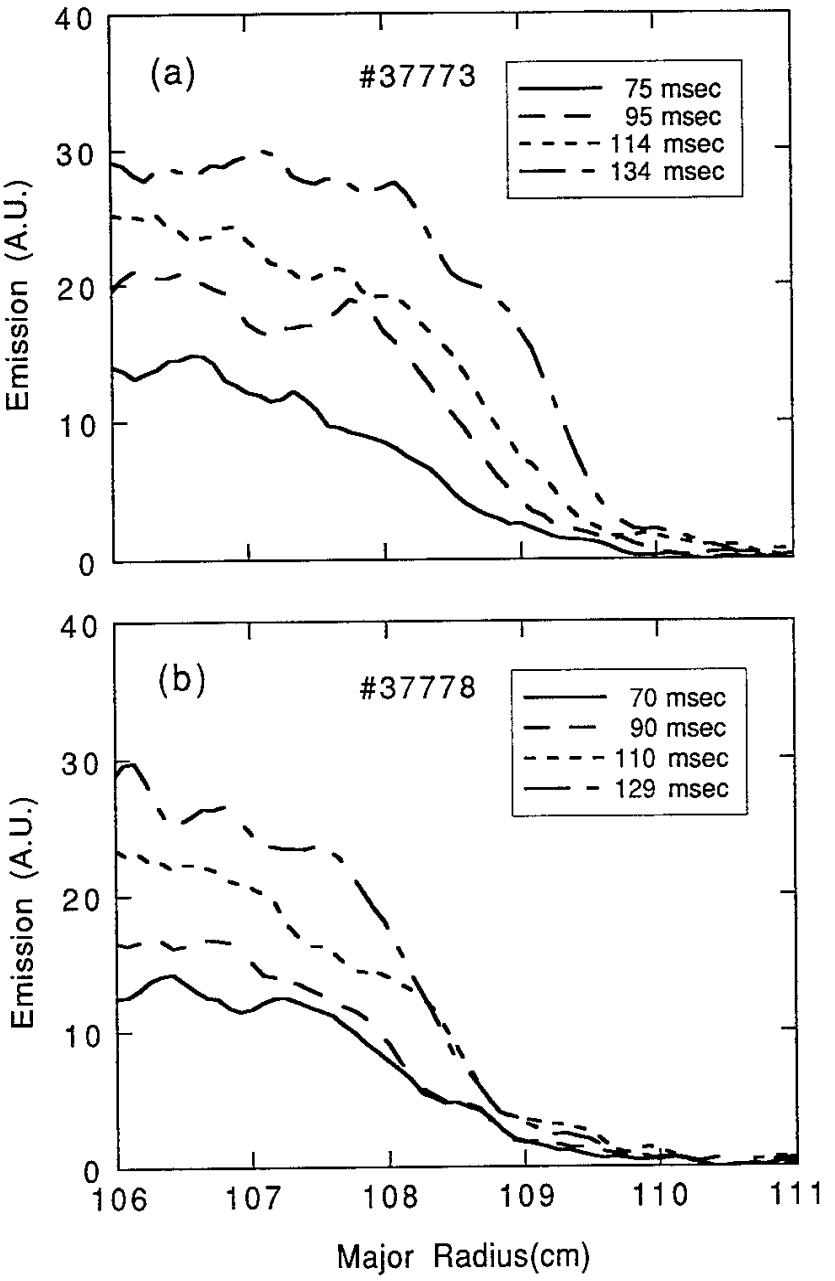

Fig. 9 Time evolutions of VUV emission profiles for (a) no variation of poloidal coil currents and (b) dynamic poloidal field control.

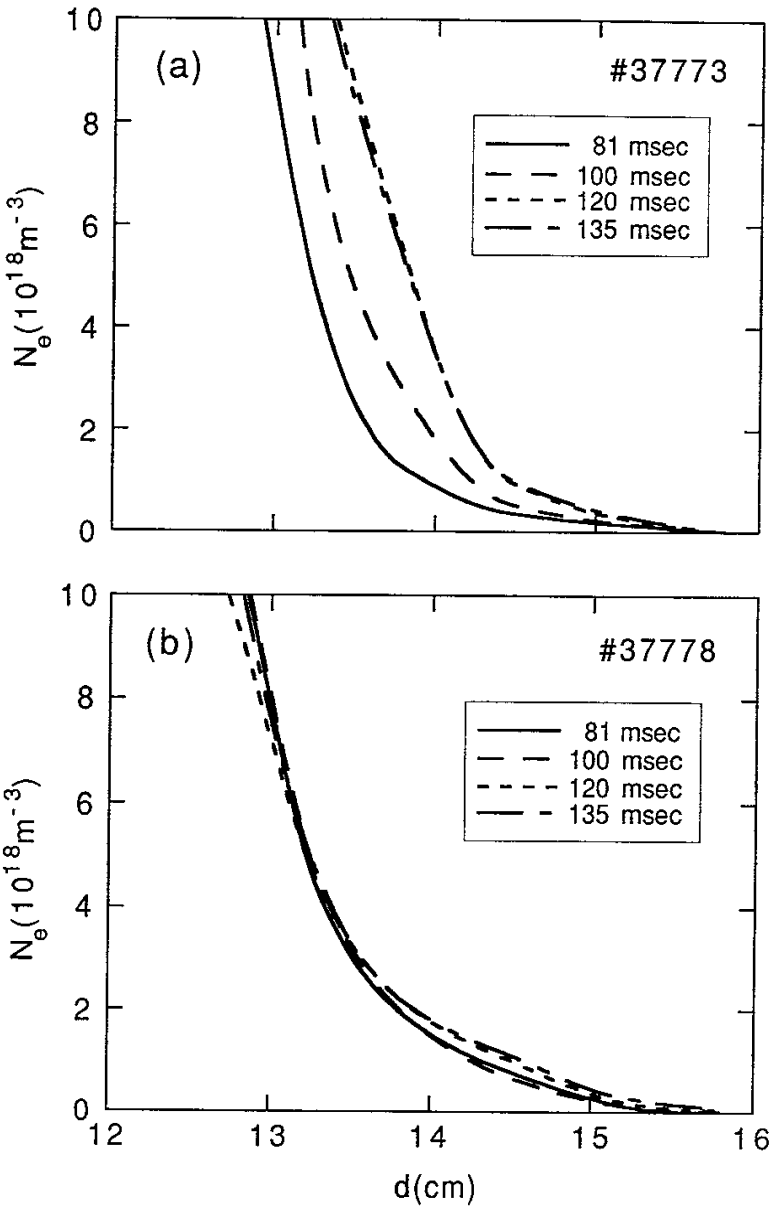

Fig. 10 Time evolutions of edge density profiles measured with lithium beam probe for (a) no variation of poloidal coil currents and (b) dynamic poloidal field control.

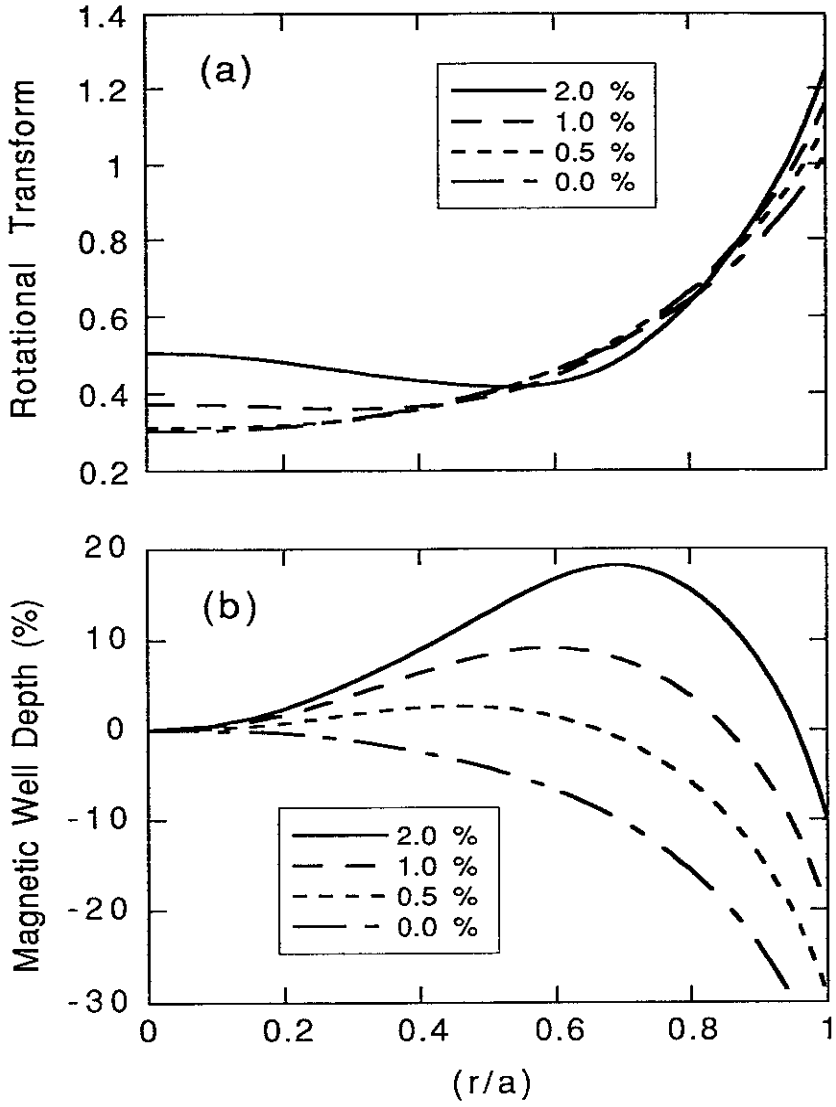

Fig. 11 Radial profiles of (a) rotational transform, (b) magnetic well obtained from free-boundary VMEC equilibrium calculations for $R_{ax} = 92$ cm configuration. Four selected equilibria are plotted for $\langle\beta\rangle = 0$ %, 0.5 %, 1 % and 2 %. Pressure profile is assumed to be proportional to $p(0)\,(1-(r/a)^{1.7})^{1.5}$ for each equilibrium.

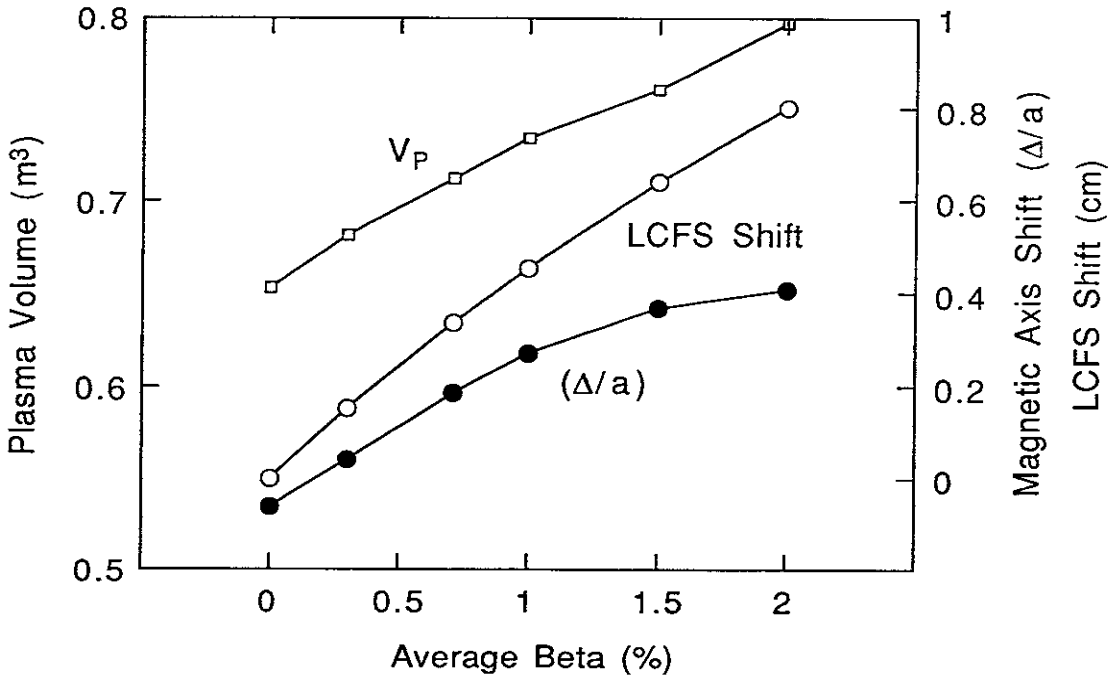

Fig. 12 Calculated values of expansion of plasma volume, shift of last closed flux surface (LCFS) at the toroidal position where the magnetic surfaces are vertically elongated and the ratio of magnetic axis shift to minor ratius (Δ/a) as functions of average beta.

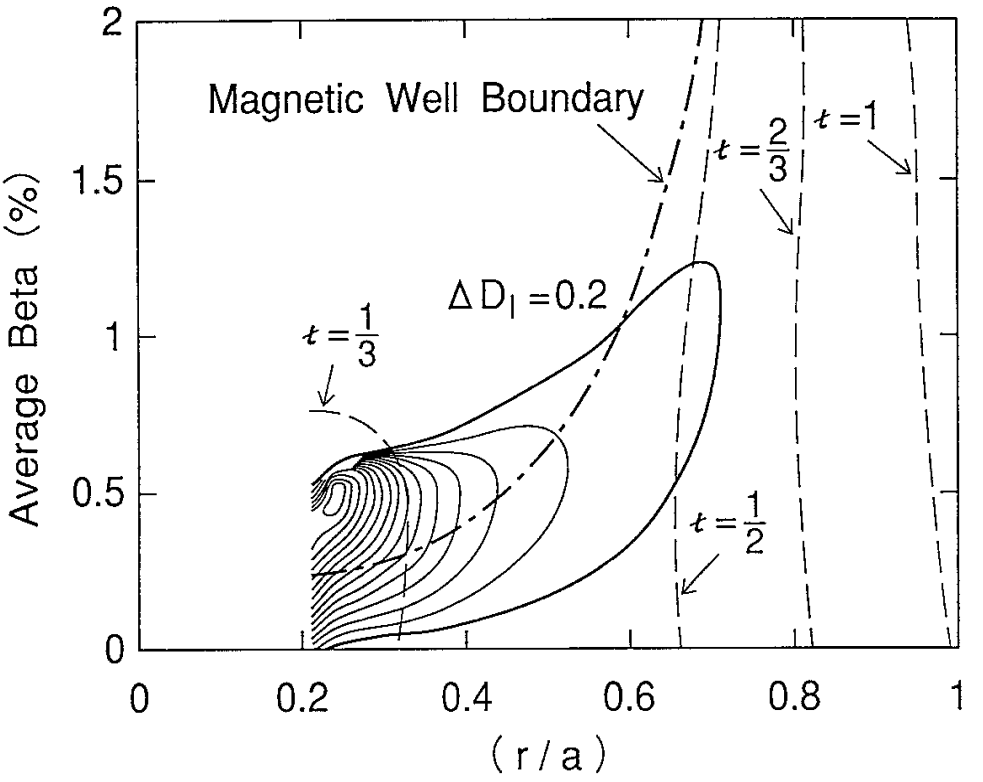

Fig. 13 Contour map of normalized Mericier stability criterion D_I obtained from free-boundary VMEC equilibrium calculations for $R_{ax} = 92$ cm configuration. Thick solid line gives Mercier stability boundary : $D_I = 0$. Thinner lines give contours with steps $\Delta D_I = 0.2$.

Recent Issues of NIFS Series

NIFS-233 R. Horiuchi and T. Sato, *Collisionless Driven Magnetic Reconnection,* June 1993

NIFS-234 K. Itoh, S.-I. Itoh, A. Fukuyama, M. Yagi and M. *Azumi, Prandtl Number of Toroidal Plasmas;* June 1993

NIFS-235 S. Kawata, S. Kato and S. Kiyokawa , *Screening Constants for Plasma;* June 1993

NIFS-236 A. Fujisawa and Y. Hamada, *Theoretical Study of Cylindrical Energy Analyzers for MeV Range Heavy Ion Beam Probes;* July 1993

NIFS-237 N. Ohyabu, A. Sagara, T. Ono, T. Kawamura and O. Motojima, *Carbon Sheet Pumping;* July 1993

NIFS-238 K. Watanabe, T. Sato and Y. Nakayama, *Q-profile Flattening due to Nonlinear Development of Resistive Kink Mode and Ensuing Fast Crash in Sawtooth Oscillations;* July 1993

NIFS-239 N. Ohyabu, T. Watanabe, Hantao Ji, H. Akao, T. Ono, T. Kawamura, K. Yamazaki, K. Akaishi, N. Inoue, A. Komori, Y. Kubota, N. Noda, A. Sagara, H. Suzuki, O. Motojima, M. Fujiwara, A. Iiyoshi, *LHD Helical Divertor;* July 1993

NIFS-240 Y. Miura, F. Okano, N. Suzuki, M. Mori, K. Hoshino, H. Maeda, T. Takizuka, JFT-2M Group, K. Itoh and S.-I. Itoh, *Ion Heat Pulse after Sawtooth Crash in the JFT-2M Tokamak;* Aug. 1993

NIFS-241 K. Ida, Y.Miura, T. Matsuda, K. Itoh and JFT-2M Group, *Observation of non Diffusive Term of Toroidal Momentum Transport in the JFT-2M Tokamak;* Aug. 1993

NIFS-242 O.J.W.F. Kardaun, S.-I. Itoh, K. Itoh and J.W.P.F. Kardaun, *Discriminant Analysis to Predict the Occurrence of ELMS in H-Mode Discharges;* Aug. 1993

NIFS-243 K. Itoh, S.-I. Itoh, A. Fukuyama, *Modelling of Transport Phenomena;* Sep. 1993

NIFS-244 J. Todoroki, *Averaged Resistive MHD Equations;* Sep. 1993

NIFS-245 M. Tanaka, *The Origin of Collisionless Dissipation in Magnetic Reconnection;* Sep. 1993

NIFS-246 M. Yagi, K. Itoh, S.-I. Itoh, A. Fukuyama and M. Azumi,

Current Diffusive Ballooning Mode in Seecond Stability Region of Tokamaks; Sep. 1993

NIFS-247 T. Yamagishi,
Trapped Electron Instabilities due to Electron Temperature Gradient and Anomalous Transport; Oct. 1993

NIFS-248 Y. Kondoh,
Attractors of Dissipative Structure in Three Disspative Fluids; Oct. 1993

NIFS-249 S. Murakami, M. Okamoto, N. Nakajima, M. Ohnishi, H. Okada,
Monte Carlo Simulation Study of the ICRF Minority Heating in the Large Helical Device; Oct. 1993

NIFS-250 A. Iiyoshi, H. Momota, O. Motojima, M. Okamoto, S. Sudo, Y. Tomita, S. Yamaguchi, M. Ohnishi, M. Onozuka, C. Uenosono,
Innovative Energy Production in Fusion Reactors; Oct. 1993

NIFS-251 H. Momota, O. Motojima, M. Okamoto, S. Sudo, Y. Tomita, S. Yamaguchi, A. Iiyoshi, M. Onozuka, M. Ohnishi, C. Uenosono,
Characteristics of D-^{3}He Fueled FRC Reactor: ARTEMIS-L, Nov. 1993

NIFS-252 Y. Tomita, L.Y. Shu, H. Momota,
Direct Energy Conversion System for D-^{3}He Fusion, Nov. 1993

NIFS-253 S. Sudo, Y. Tomita, S. Yamaguchi, A. Iiyoshi, H. Momota, O. Motojima, M. Okamoto, M. Ohnishi, M. Onozuka, C. Uenosono,
Hydrogen Production in Fusion Reactors, Nov. 1993

NIFS-254 S. Yamaguchi, A. Iiyoshi, O. Motojima, M. Okamoto, S. Sudo, M. Ohnishi, M. Onozuka, C. Uenosono,
Direct Energy Conversion of Radiation Energy in Fusion Reactor, Nov. 1993

NIFS-255 S. Sudo, M. Kanno, H. Kaneko, S. Saka, T. Shirai, T. Baba,
Proposed High Speed Pellet Injection System "HIPEL" for Large Helical Device
Nov. 1993

NIFS-256 S. Yamada, H. Chikaraishi, S. Tanahashi, T. Mito, K. Takahata, N. Yanagi, M. Sakamoto, A. Nishimura, O. Motojima, J. Yamamoto, Y. Yonenaga, R. Watanabe,
Improvement of a High Current DC Power Supply System for Testing the Large Scaled Superconducting Cables and Magnets; Nov. 1993

NIFS-257 S. Sasaki, Y. Uesugi, S. Takamura, H. Sanuki, K. Kadota,
Temporal Behavior of the Electron Density Profile During Limiter

Biasing in the HYBTOK-II Tokamak; Nov. 1993

NIFS-258 K. Yamazaki, H. Kaneko, S. Yamaguchi, K.Y. Watanabe, Y.Taniguchi, O.Motojima, LHD Group,
Design of Central Control System for Large Helical Device (LHD); Nov. 1993

NIFS-259 S. Yamada, T. Mito, A. Nishimura, K. Takahata, S. Satoh, J. Yamamoto, H. Yamamura, K. Masuda, S. Kashihara, K. Fukusada, E. Tada,
Reduction of Hydrocarbon Impurities in 200L/H Helium Liquefier-Refrigerator System; Nov. 1993

NIFS-260 B.V.Kuteev,
Pellet Ablation in Large Helical Device; Nov. 1993

NIFS-261 K. Yamazaki,
Proposal of "MODULAR HELIOTRON': Advanced Modular Helical System Compatible with Closed Helical Divertor; Nov. 1993

NIFS-262 V.D.Pustovitov,
Some Theoretical Problems of Magnetic Diagnostics in Tokamaks and Stellarators; Dec. 1993

NIFS-263 A. Fujisawa, H. Iguchi, Y. Hamada
A Study of Non-Ideal Focus Properties of 30° Parallel Plate Energy Analyzers; Dec. 1993

NIFS-264 K. Masai,
Nonequilibria in Thermal Emission from Supernova Remnants; Dec. 1993

NIFS-265 K. Masai, K. Nomoto,
X-Ray Enhancement of SN 1987A Due to Interaction with its Ring-like Nebula; Dec. 1993

NIFS-266 J. Uramoto
A Research of Possibility for Negative Muon Production by a Low Energy Electron Beam Accompanying Ion Beam; Dec. 1993

NIFS-267 H. Iguchi, K. Ida, H. Yamada, K. Itoh, S.-I. Itoh, K. Matsuoka, S. Okamura, H. Sanuki, I. Yamada, H. Takenaga, K. Uchino, K. Muraoka,
The Effect of Magnetic Field Configuration on Particle Pinch Velocity in Compact Helical System (CHS); Jan. 1994

NIFS-268 T. Shikama, C. Namba, M. Kosuda, Y. Maeda,
Development of High Time-Resolution Laser Flash Equipment for Thermal Diffusivity Measurements Usting Miniature-Size Specimens; Jan. 1994

NIFS-269 T. Hayashi, T. Sato, P. Merkel, J. Nührenberg, U. Schwenn,
Formation and 'Self-Healing' of Magnetic Islands in Finite-β Helias Equilibria; Jan. 1994

NIFS-270 S. Murakami, M. Okamoto, N. Nakajima, T. Mutoh,
Efficiencies of the ICRF Minority Heating in the CHS and LHD Plasmas; Jan. 1994

NIFS-271 Y. Nejoh, H. Sanuki,
Large Amplitude Langmuir and Ion-Acoustic Waves in a Relativistic Two-Fluid Plasma; Feb. 1994

NIFS-272 A. Fujisawa, H. Iguchi, A. Taniike, M. Sasao, Y. Hamada,
A 6MeV Heavy Ion Beam Probe for the Large Helical Device;
Feb. 1994

NIFS-273 Y. Hamada, A. Nishizawa, Y. Kawasumi, K. Narihara, K. Sato, T. Seki, K. Toi, H. Iguchi, A. Fujisawa, K. Adachi, A. Ejiri, S. Hidekuma, S. Hirokura, K. Ida, J. Koong, K. Kawahata, M. Kojima, R. Kumazawa, H. Kuramoto, R. Liang, H. Sakakita, M. Sasao, K. N. Sato, T. Tsuzuki, J. Xu, I. Yamada, T. Watari, I. Negi,
Measurement of Profiles of the Space Potential in JIPP T-IIU Tokamak Plasmas by Slow Poloidal and Fast Toroidal Sweeps of a Heavy Ion Beam; Feb. 1994

NIFS-274 M. Tanaka,
A Mechanism of Collisionless Magnetic Reconnection; Mar. 1994

NIFS-275 A. Fukuyama, K. Itoh, S.-I. Itoh, M. Yagi and M. Azumi,
Isotope Effect on Confinement in DT Plasmas; Mar. 1994

NIFS-276 R.V. Reddy, K. Watanabe, T. Sato and T.H. Watanabe,
Impulsive Alfven Coupling between the Magnetosphere and Ionosphere, Apr.1994

NIFS-277 J. Uramoto,
A Possibility of π^- Meson Production by a Low Energy Electron Bunch and Positive Ion Bunch, Apr. 1994

NIFS-278 K. Itoh, S.-I. Itoh, A. Fukuyama, M. Yagi and M. Azumi,
Self-sustained Turbulence and L-mode Confinement in Toroidal Plasmas II, Apr. 1994

NIFS-279 K. Yamazaki and K.Y.Watanabe,
New Modular Heliotron System Compatible with Closed Helical Divertor and Good Plasma Confinement, Apr. 1994